Available online at www.sciencedirect.com
ScienceDirect
Trans. Nonferrous Met. Soc. China 27(2017) 1794−1803
Transactions of Nonferrous Metals Society of China
www.tnmsc.cn

Effect of bismuth tungstate with different hierarchical architectures on photocatalytic degradation of norfloxacin under visible light

Jia-jia WANG[1,2], Lin TANG[1,2], Guang-ming ZENG[1,2], Yao-yu ZHOU[3], Yao-cheng DENG[1,2], Chang-zheng FAN[1,2], Ji-lai GONG[1,2], Ya-ni LIU[1,2]

1. College of Environmental Science and Engineering, Hunan University, Changsha 410082, China;
2. Key Laboratory of Environmental Biology and Pollution Control, Ministry of Education, Hunan University, Changsha 410082, China;
3. College of Resources and Environment, Hunan Agricultural University, Changsha 410128, China

Received 13 April 2016; accepted 28 December 2016

Abstract: The photocatalytic degradation of norfloxacin by bismuth tungstate (Bi_2WO_6) with different hierarchical architectures was investigated under visible light irradiation. Bi_2WO_6 was prepared by hydrothermal method with the reaction solution pH ranging from 4 to11. The relatively ultrathin Bi_2WO_6 nanoflakes prepared at pH 4 showed excellent adsorption and photodegradation efficiency towards norfloxacin. The characterization results showed that Bi_2WO_6 prepared at pH 4 had a larger specific area and faster photo-generated carrier separation rate. The decay rate reached the maximum in weak alkaline reaction solution, which could be attributed to the presence of moderate OH^- anions. The present study demonstrated that the smaller size of Bi_2WO_6 could be an efficient photocatalyst on the degradation of norfloxacin in the aquatic environment.

Key words: norfloxacin; bismuth tungstate; hierarchical architecture; photocatalytic degradation; size effect

1 Introduction

The frequent occurrence of pharmaceuticals in the aquatic environment has become an important issue in past decades [1−3]. Particularly after HIRSCH et al [2] separated antibiotic resistant bacteria from sewage sludge, and NEU [4] reported the crisis in antibiotic resistance of microorganisms, the focus turned to the occurrence of antibiotic drugs in aquatic environment. Most of the antibiotic drugs are not well adsorbed in the subsoil because of their polar structure, and may seep into groundwater aquifers from polluted surface water [5]. Among the antibiotic drugs, fluoroquinolone is synthetic and widely used in human and veterinary medicine. Recently, fluoroquinolone reserved in sewage water, surface water and ground water has been reported to lead to an obviously adverse effect on the aquatic ecosystems [6−11]. Norfloxacin is one of the main fluoroquinolone antibiotics, and 75% of it is excreted from the human body and remain unchanged [12].

In the past decade, researchers have explored the removal of pharmaceutical compounds in aqueous systems by different methods, including adsorption [13], biodegradation [14], ultrasonic [15] and chemical techniques [16]. Carbonaceous absorbents can quickly adsorb antibiotics and heavy metals from water due to their high pore volume and specific surface area [17−20], but there is a potential risk of the "removed" antibiotics and heavy metals being released into aquatic environment if the used sorbent is improperly disposed. Biodegradation method usually takes a long time and depends on many environmental factors such as bacterial counts, salinity, and temperature [21,22]. Among these methods, photocatalysis technique was found to be an effective method with high degradation and mineralization efficiency [23−25]. Since the discovery of the photocatalytic splitting of H_2O on the TiO_2 electrodes by FUJISHIMA et al [26], TiO_2 has been widely used in sterilization, sanitation, and remediation

Foundation item: Projects (51579096, 51222805, 51521006, 51508175) supported by the National Natural Science Foundation of China; Project supported by the National Program for Support of Top-Notch Young Professionals of China; Project (NCET–11–0129) supported by the Program for New Century Excellent Talents in University from the Ministry of Education of China; Project (CX2015B095) supported by the Hunan Province Innovation Foundation for Postgraduate, China

Corresponding author: Lin TANG; Tel: +86-731-88822778; Fax: +86-731-88823701; E-mail: tanglin@hnu.edu.cn

DOI: 10.1016/S1003-6326(17)60202-4

applications [27−29], providing a promising method for water treatment. However, the widely used photocatalyst, namely TiO_2, can only be excited by UV light with an irradiation wavelength less than 380 nm, which significantly limits its application. Therefore, it is urgent to develop highly efficient visible-light induced photocatalysts to meet the high requirements in dealing with environmental antibiotic pollution in the future.

Bismuth tungstate is a new kind of photocatalyst, and has been proved to have efficient performance in the solar-light-mediated systems [30]. Our previous work demonstrated that Bi_2WO_6 could efficiently photodegrade norfloxacin under the assistance of surfactant [31]. Bi_2WO_6 can absorb visible light in wider area (λ=400−800 nm) and has a photonic band gap (E_g=2.72 eV) narrower than that of TiO_2. The photocatalytic capability of Bi_2WO_6 is attributed to the band transition from the hybrid orbitals of Bi 6s and O 2p to the W 5d orbitals. Although the potential advantages of Bi_2WO_6 on photocatalysis have been discovered, the study on photocatalytic degradation of antibiotic norfloxacin using the Bi_2WO_6 with different morphologies and hierarchical architectures was rarely reported. The decomposition of organic contaminants in wastewater using the irradiated photocatalyst was explored [32], and the schemes are given as follows:

$$Bi_2WO_6+h\nu \longrightarrow Bi_2WO_6+h^++e \quad (1)$$

$$O_2+e \longrightarrow O_2\bullet^- \quad (2)$$

$$H_2O+h^+ \longrightarrow \bullet OH+H^+ \quad (3)$$

Bi_2WO_6 has different morphologies and hierarchical architectures made up of different sizes of nano-crystals. With the change of crystal size, quantum size effect and good physicochemical property such as high specific area may occur on photocatalyst. They are beneficial to improving the photodegradation of contaminants in the aquatic environment. It is necessary to specifically investigate the effect of different hierarchical architectures of Bi_2WO_6 on photocatalysis of antibiotics, which was seldom studied in the literature. We chose norfloxacin as the target pollutant (shown in Fig. 1).

This work aimed to study the photocatalytic degradation effect of norfloxacin by Bi_2WO_6 with different hierarchical architectures under visible light. Bi_2WO_6 catalysts were synthesized using hydrothermal method with different morphologies by varying the pH values of the reaction solutions. The physicochemical properties of the prepared catalysts were characterized, and their degradation capacities of norfloxacin were investigated. The impacts of different reaction factors on the degradation efficiency of the prepared catalyst were also discussed.

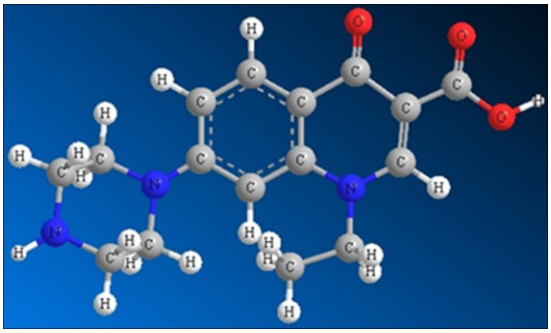

Fig. 1 Molecule structure of norfloxacin

2 Experimental

2.1 Materials

Norfloxacin (purity 99.8%) was purchased from Aladdin Reagent Company, Shanghai, China. All reagents used in the experiment were of analytical reagent grade. Solutions were prepared with high-purity water (18.25 MΩ/cm) from a Milli-Q water purification system.

2.2 Preparation and characterization of photocatalyst Bi_2WO_6

2.2.1 Preparation of photocatalyst Bi_2WO_6

Bi_2WO_6 samples were synthesized using hydrothermal method according to Ref. [33]. In general, 0.97 g of $Bi(NO_3)_3\cdot 5H_2O$ was dissolved into 20 mL of 1.0 mol/L HNO_3. 0.33 g of $Na_2WO_4\cdot 2H_2O$ was dissolved into the same volume of 1.0 mol/L NaOH. Then, the mixed solution was mixed ultrasonically at room temperature for 30 min. The pH value of reaction solution was adjusted to 4, 7, 9, and 11, respectively. Then, the suspension was transferred into a 100 mL Teflon-lined autoclave, and heated at 140 °C for 20 h. The obtained precipitates were washed with water and ethanol several times, and finally dried at 120 °C for 4 h. The obtained samples were denoted as Bi_2WO_6-pH4, Bi_2WO_6-pH7, Bi_2WO_6-pH9 and Bi_2WO_6-pH11, respectively.

2.2.2 Characterization

Crystallographic information of Bi_2WO_6 was obtained by X-ray diffraction (XRD, 43 Rigaku D/MAX-RB, Cu K_α radiation, Japan). The morphology of the prepared samples was observed by a 1530VP scanning electron microscope (SEM, Quanta 200 FEG, FEI Company, America). The specific surface area was measured by a Quantachrome NOVA 2000e sorption analyzer (Quantachrome, America). UV–Vis diffused reflectance spectra (DRS, Shimadzu, UV−3150, Japan) of Bi_2WO_6 were obtained on a Hitachi U−3010 spectrometer, using $BaSO_4$ as the reference.

2.3 Norfloxacin degradation procedures

The degradation experiment was carried out under

visible light of a 300 W Xe lamp (CEL-HXF300 Zhongjiaojinyuan, Beijing, China) with a 400 nm cut off filter. Solutions with certain concentrations of norfloxacin were prepared in high-purity water. Aqueous solution of norfloxacin was dissolved in 1 L of high purity water by adding 0.5 mL of 1 mol/L NaOH solution to increase its solubility. In each experiment, the prepared Bi_2WO_6 was added into 100 mL of 20 mg/L norfloxacin solution. Prior to irradiation, reaction solution was magnetically stirred in the dark for 20 min. 1 mL of reaction solution was withdrawn at preset intervals and filtered through 13 mm × 0.45 μm membrane for norfloxacin analysis.

2.4 Analysis

The norfloxation concentrations were quantitatively determined by a UV−Vis spectrophotometer (Shimazdu, UV 2100) at 280 nm, the wavelength for the maximum absorption peak of norfloxacin.

3 Results and discussion

3.1 Characterization of Bi_2WO_6 prepared at different hydrothermal pH values

XRD patterns of Bi_2WO_6 prepared at different hydrothermal pH values are shown in Fig. 2, indicating that the crystal structure is Bi_2WO_6 crystal phase with orthorhombic symmetry. It features a higher peak centered at 2θ of about 28° and a lower peak at 2θ around 33°. The diffraction peaks of the product are in accordance with those of russellite Bi_2WO_6 (JCPDS No. 39-0256). However, new crystal phases emerge when hydrothermal pH increases to 11. The intensity of the highest peak (131) increases as pH varied from 4 to 9, indicating an enhancement in crystallinity perfection and formation of larger Bi_2WO_6 crystallites. The crystallite size was calculated by the Debye−Scherrer equation as follows, with the results shown in Table 1.

$$d=0.89\lambda/(B\cos\theta) \quad (4)$$

where λ is the X-ray wavelength, θ is the angle of Bragg diffraction, and B is the difference between the full width at half maximum and the instrumental broadening.

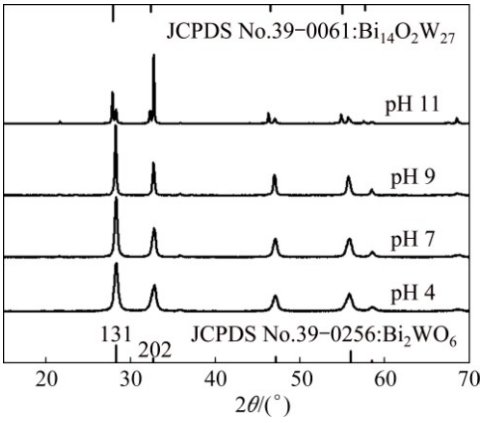

Fig. 2 XRD patterns of catalysts prepared at different pH values

Table 1 Characteristics of Bi_2WO_6 prepared at different hydrothermal pH values

pH	Crystallite size/nm	S_{BET}/($m^2\cdot g^{-1}$)	Pore size/nm
4	12.5−14.4	20.6	37.0
7	15.8−19.2	11.4	32.4
9	26.5−31.7	7.1	37.2
11	29.9−40.1	5.6	46.9

The morphologies of the catalysts were further characterized by SEM (Fig. 3). The hydrothermal pH had a strong effect on the morphologies of the catalysts. As shown in Fig. 3, Bi_2WO_6-pH4 has a persimmon cake-like hierarchical architecture with regular size assembled by ultrathin nanoflakes. At pH 7, nanoflakes in larger aggregates (about 2 μm in size) with irregular shape and uneven size are visible. At pH 9, rectangular sheets with some aggregated fragments or particles appear. And at pH 11, its morphology is mainly composed of a mixture of small spherical particles and large sheets (about 3 μm in size), which implies that the Bi_2WO_6-pH11 has different compositions. These results agreed well with the increase of crystallite size in XRD study. The specific surface area of the small spherical particles emerged at higher preparation pH is relatively small [34]. As a result, the specific surface area decreased with the increase of the pH value.

Bi_2WO_6-pH4 has the largest specific surface area, which is attributed to the thinner and smaller platelets. As shown in Table 1, the S_{BET} decreased gradually from 20.6 to 11.4, 7.1 and 5.6 m^2/g at pH values of 4, 7, 9 and 11, respectively.

Bismuth tungsten oxide was proposed to grow in supersaturated Na_2WO_4 and $Bi(NO_3)_3$ solution, and amorphous fine particles acted as the precursor for the synthesis of crystal Bi_2WO_6 [35]. The relevant chemical reactions can be formulated [36]. When the pH value of the precursor solution is low (≤7), the reactions are illustrated as follows:

$$Na_2WO_4\cdot 2H_2O+2HNO_3\longrightarrow 2H_2WO_4\downarrow+2NaNO_3+2H_2O \quad (5)$$

$$Bi(NO_3)_3+H_2O\rightleftharpoons BiONO_3+2HNO_3 \quad (6)$$

$$2Bi(NO_3)_3+3H_2O\rightleftharpoons Bi_2O_2(OH)NO_3+5HNO_3 \quad (7)$$

$$Bi_2O_2(OH)NO_3+H_2WO_4\longrightarrow Bi_2WO_6+HNO_3+H_2O \quad (8)$$

$$2BiONO_3+H_2WO_4\longrightarrow Bi_2WO_6+2HNO_3 \quad (9)$$

Under the alkaline condition (pH>7), the reaction is illustrated as follows:

$$7Bi_2O_2(OH)NO_3+2WO_4^{2-}+3OH^-\longrightarrow Bi_{14}W_2O_{27}+7NO_3^-+5H_2O \quad (10)$$

The formation of Bi_2WO_6 samples with different hierarchical architectures could be described in Fig. 4. It

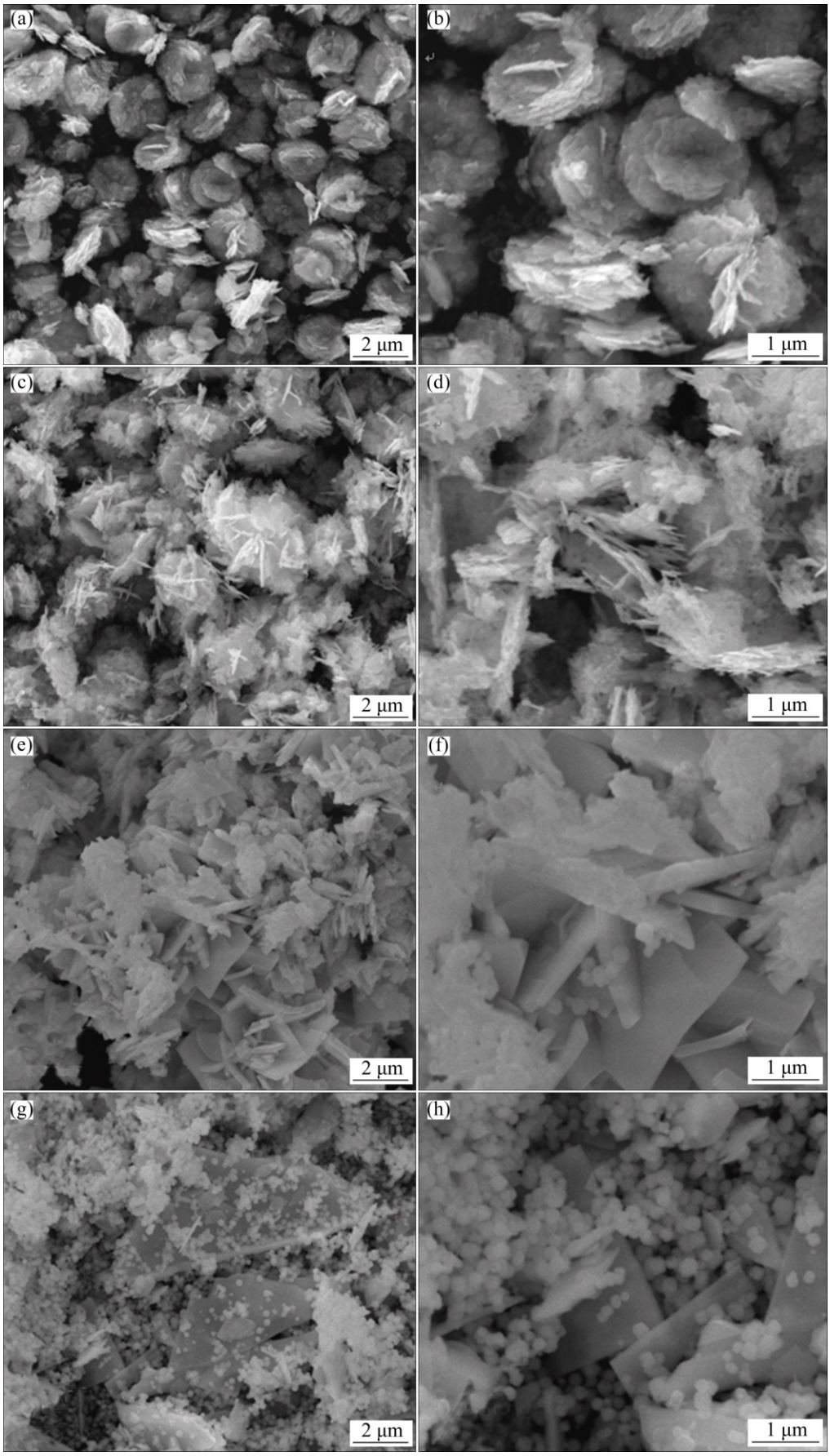

Fig. 3 SEM images of Bi_2WO_6-pH4 (a, b), Bi_2WO_6-pH7 (c, d), Bi_2WO_6-pH9 (e, f), and Bi_2WO_6-pH11 (g, h)

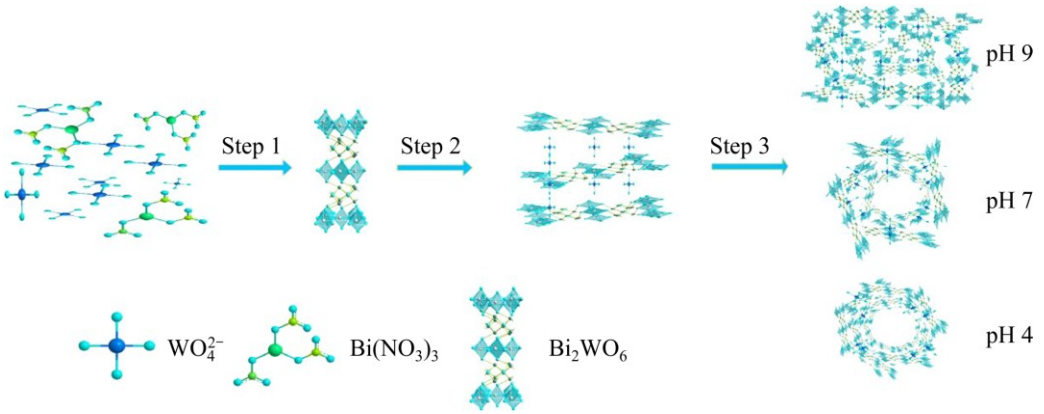

Fig. 4 Schematic diagram of crystal growth mechanism for Bi_2WO_6

involves nucleation, oriented attachment, and self-assembly process [35]. The formation of different hierarchical architectures of bismuth tungstate in each intermediate process was demonstrated by ZHANG et al [37] by SEM. As depicted above, the pH value of precursor solution has a strong influence on the formation of slightly soluble H_2WO_4, which further determines the rates of nucleation and the assembly manners of Bi_2WO_6 platelets [38]. In the acidic conditions (pH≤7), the richly formed H_2WO_4 precipitate would react with rapidly hydrolyzing $Bi(NO_3)_3$, which substantially promoted the nucleation of Bi_2WO_6. The large number of nucleation centers of Bi_2WO_6 benefited the formation of the persimmon cake-like Bi_2WO_6 hierarchical nano/microstructures. In alkaline conditions (pH>7), the yield of H_2WO_4 precipitate decreased, which benefited the preferential growth of large rectangular platelets of Bi_2WO_6. However, as the pH value increased to 11, the $Bi_{14}W_2O_{27}$ phase began to dominate.

As is known, optical absorption by photocatalyst materials and migration of the light-induced electrons (e) and holes (h^+) are determined by their electronic structure features which play an important role in affecting their photocatalytic activity. In the UV–Vis diffuse reflectance spectrum (DRS) analysis (Fig. 5), it was found that all the Bi_2WO_6 samples had a strong broad background light absorption in the range from UV-light to visible light around 450 nm and showed an absorption edge around 450 nm, suggesting their potential photocatalytic activity under visible light. The steep shape of the spectra was observed, indicating that the visible-light absorption was not due to the transition from the impurity level, but due to the band gap transition [39]. The band gap energies of semiconductors can be estimated by Kubelka−Munk transformation, $\alpha h\upsilon=A(h\upsilon-E_g)^{n/2}$, where α represents the absorption coefficient; υ is the light frequency; E_g is the band gap energy; A is a constant, and n depends on the characteristics of the transition in a semiconductor. According to Kubelka−Munk transformation, E_g values of Bi_2WO_6 samples prepared at pH 4, 7, 9 and 11 were calculated to be 2.69, 2.73, 2.73 and 2.76 eV, respectively (inset of Fig. 5).

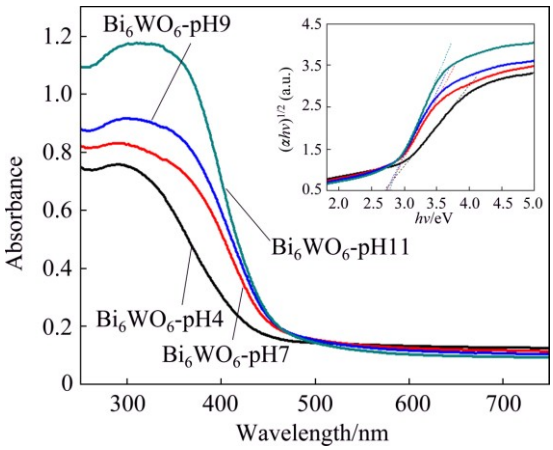

Fig. 5 UV−Vis diffuse reflectance and band gap of prepared catalysts

3.2 Degradation efficiency of catalysts with different hierarchical architectures

To investigate the influence of degradation efficiency of Bi_2WO_6 with different hierarchical architectures, we put the hydrothermally synthesized catalysts at pH 4, 7, 9 and 11 into 100 mL of 20 mg/L norfloxacin solution, respectively. The concentration of catalyst in the solution was set at 1.0 g/L. Before irradiation, each adsorption experiment was firstly conducted in the dark for 60 min, shown in Fig. 6(a). The adsorption quickly reached equilibrium within 20 min. The adsorption capacity of Bi_2WO_6 prepared in specific hydrothermal conditions decreased as the pH of hydrothermal solution increased. About 50% norfloxacin could be adsorbed by Bi_2WO_6-pH4, while only about 10% was adsorbed by Bi_2WO_6-pH11. The results were mainly attributed to their different surface areas (shown in Table 1). Bi_2WO_6-pH4 had the largest surface area

among those catalysts, providing more adsorption sites for norfloxacin.

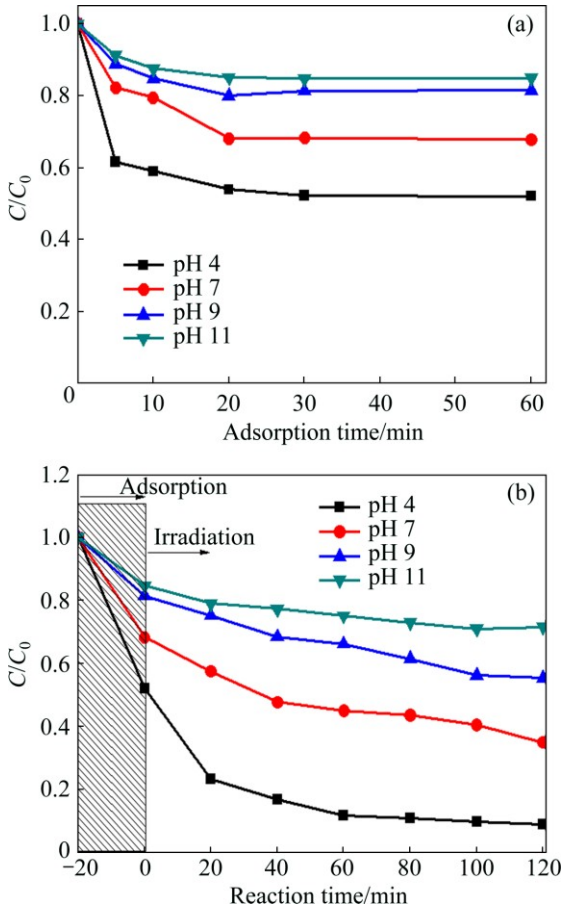

Fig. 6 Adsorption of norfloxacin on Bi_2WO_6 prepared at different hydrothermal pH values (a) and degradation of norfloxacin by Bi_2WO_6 prepared at different hydrothermal pH values (b)

As shown in Fig. 6(b), it was interestingly found that the persimmon cake-like hierarchical architecture of Bi_2WO_6-pH4 also displayed the highest degradation efficiency to norfloxacin, and the photodegradation efficiency decreased when the hydrothermal pH increased from 4 to 11. The photocatalytic degradation almost reached equilibrium within 60 min. Almost 90% of norfloxacin was decomposed by Bi_2WO_6-pH4, while only 20% norfloxacin was degraded by Bi_2WO_6-pH11, indicating that the newly emerged crystal phases at higher hydrothermal pH had less photocatalytic activity in degradation of norfloxacin. Furthermore, the kinetic curves of norfloxacin photodegradation can be approximated as a pseudo-first-order process [40]:

$$\ln\frac{C_t}{C_0} = -K_{obs}t \quad (11)$$

where K_{obs} represents the apparent degradation rate constant. The K_{obs} of norfloxacin photodegration by Bi_2WO_6-pH4 is 0.0133 min^{-1}, which is 2.77, 3.91 and 9.50 times as much as those of Bi_2WO_6-pH7 (0.0048 min^{-1}), Bi_2WO_6-pH9 (0.0034 min^{-1}), and Bi_2WO_6-pH11 (0.0014 min^{-1}), respectively.

The difference in degradation rate constant could be ascribed to the different hierarchical architectures of Bi_2WO_6. Previous researchers found that surface area and crystallinity are the most important factors to influence the photocatalytic activity [41]. In our study, the hierarchical architecture of Bi_2WO_6 synthesized at lower pH exhibited large specific surface area with relatively inferior crystallite (see Fig. 2). It has been reported that electron−hole recombination on the particle surface would be reduced by an increase in surface defects [42]. According to the XRD (Fig. 2) and SEM (Fig. 3), the smaller and the thinner the platelets are, the larger the surface area the nanoflakes have, and they can provide more active sites which enhance photocatalytic activity. So, the persimmon cake-like hierarchical architecture of Bi_2WO_6 exhibited the highest photocatalytic activity. The S_{BET} value of Bi_2WO_6-pH4 is also far more than those of the other samples. The degradation efficiency of contaminant decreased with a downtrend of the S_{BET} of the catalyst as the hydrothermal pH increased from 4 to 11. Herein, we selected Bi_2WO_6-pH4 for further study and discussed in detail in the following sections.

3.3 Effect of catalyst dosage

The influence of the photocatalyst dosage on norfloxacin degradation was studied in 20 mg/L norfloxacin solution at pH 9 as shown in Fig. 7. The photocatalytic degradation efficiency of norfloxacin increased drastically with the increase of photocatalyst dosage from lower amount to 1.0 g/L, but then decreased slightly with photocatalyst dosage increasing from 1.0 to 2.0 g/L. It is possibly due to the penetration of photoactivating light into the suspension that was reduced at excessive catalyst dosage. The availability of active sites increased with the increasing catalyst dosage in the suspension, while the light penetration and the photoactivated volume of the suspension decreased. Furthermore, agglomeration and sedimentation of the Bi_2WO_6 particles in suspension may also affect the reaction between photocatalyst and contaminant [43]. Under this circumstance, part of the catalyst surface becomes unavailable for photon absorption and contaminant adsorption, thus hindering the catalytic reaction. The dosing amount of Bi_2WO_6 should be optimized in order to ensure adequate absorption of light photons for efficient photodegradation. As shown in Fig. 7, 1.0 g/L Bi_2WO_6 can provide sufficient catalyst activity without hindering light penetration.

3.4 Effects of initial pH

The initial pH of the norfloxacin solution could have a significant effect on the degradation. The concentration of hydrogen ions (H^+) or hydroxide ions (OH^-) in aqueous solution might affect the active sites on the surface of most photocatalysts. Hydroxide ions could react with hole (h^+) to generate reactive species •OH radicals, hence enhancing the photocatalytic activity. Mechanically, •OH is believed to be a strong oxidant for organic contaminants in the photocatalytic process [44]. The number of e/h^+ on the photocatalyst surface plays an important role in determining the photocatalytic reaction rate. The generation of •OH depends on the solution pH value. In an alkaline solution, the generation of the radical •OH is much easier than that in neutral and acidic solutions due to much more OH^- ions in aqueous solution. Therefore, the influence of pH in the range from 3 to 11 in aqueous suspensions of Bi_2WO_6 on the degradation of norfloxacin was studied. Figure 8 shows the degradation rate of norfloxacin by employing Bi_2WO_6. The maximum degradation rate of norfloxacin occurred at alkaline pH (pH 9), and both the lower and higher pH values resulted in decreasing degradation rate.

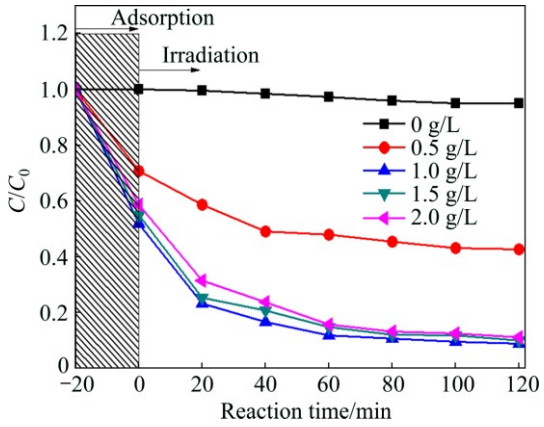

Fig. 7 Degradation of norfloxacin with different dosages of Bi_2WO_6 at initial pH of 9

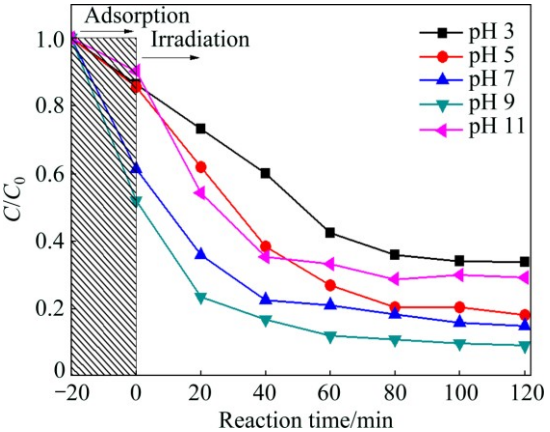

Fig. 8 Degradation of norfloxacin at different initial pH values of solution and Bi_2WO_6 dosage of 1 g/L

The observed results were also closely related to the electrostatic interactions between the substrate and the photocatalyst surface which depended on the pH of the suspension [45]. Norfloxacin has two relevant ionizable functional groups: the 3-carboxyl group and N4 of the piperazine substituent. The two ionizable groups lead to two ionization constants: pK_{a1} (pH 6.34) and pK_{a2} (pH 8.75). The isoelectric point of the employed Bi_2WO_6 was measured to be pH 4.56. Under acidic conditions, norfloxacin and Bi_2WO_6 were both dominated by positive charge. The electrostatic repulsive effect between them hinders the approach of norfloxacin to the Bi_2WO_6 surface, retarding the degradation of norfloxacin. At a pH level between pK_{a1} and pK_{a2}, the main species of norfloxacin possess both negatively and positively charged sites that are accessible to negative charged Bi_2WO_6. Besides, Bi_2WO_6 transformed to H_2WO_4 and Bi_2O_3 in acidic solution, leading to lower photocatalytic activity of Bi_2WO_6 [46]. Optimal norfloxacin decay rate was observed at pH 9, which was slightly beyond the pK_{a2} probably due to the existence of more hydroxyl anions, resulting in the generation of more hydroxyl radicals and faster photocatalytic reaction. At pH 11, the decay rate decreased probably because of the repellent force between negatively charged norfloxacin and Bi_2WO_6.

Therefore, the degradation efficiency of norfloxacin in this study was significantly influenced by the pH value of solution. The high degradation efficiency of norfloxacin in alkaline pH depends on the generation of more radical •OH, the efficient adsorption of norfloxacin on catalyst surface as well as the stable crystal structure of Bi_2WO_6.

3.5 Effect of initial norfloxacin concentration

From the perspective of application, it is important to study the dependence of photocatalytic reaction on the substrate concentration. Hence, the influence of norfloxacin concentration on the degradation rate was studied in a solution at initial pH value of 9 and catalyst dosage of 1 g/L. The degradation rates for norfloxacin at different concentrations are shown in Fig. 9. It was found that lower initial concentration led to higher removal efficiency of norfloxacin, i.e., when the norfloxacin increased from 10 to 50 mg/L, the adsorption percentage on the catalyst decreased from about 55% to 2%, and the final photocatalytic degradation rate decreased from 95% to 10%. This suggested that the high adsorption rate of norfloxacin at lower concentration could contribute to the degradation rate of the contaminant. What's more, the continuous increase of the contaminant amount may cause the increase of light scattering and decrease of light penetration, resulting in low photocatalytic efficiency.

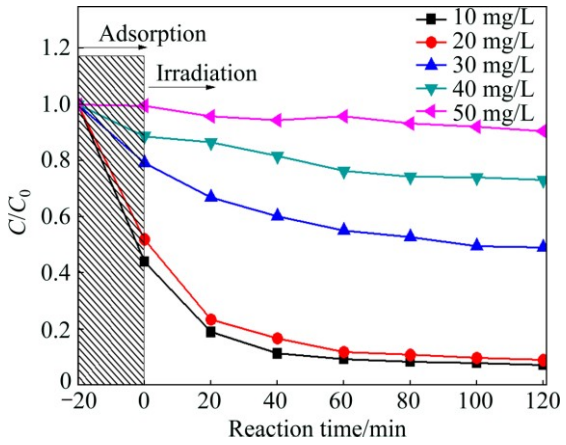

Fig. 9 Degradation of norfloxacin with various initial concentrations at Bi_2WO_6 dosage of 1 g/L and initial pH of 9

3.6 Effect of electron acceptor

In the photocatalytic reaction, the undesired electron−hole recombination is one of the troublesome problems. A good solution to avert electron–hole pair recombination is to introduce other (irreversible) electron acceptor in the reaction. A proper electron acceptor or donor would offset the major energy wasting step and further limit the achievable quantum yield. H_2O_2 was found to be a better electron acceptor than oxygen [47,48], and could reduce the chances of electron–hole recombination on the Bi_2WO_6 surface. Therefore, more hydroxyl radicals could take part in the oxidation of norfloxacin, as shown in Eq. (10). We investigated the degradation rates of norfloxacin in photocatalytic reaction with or without additional oxidant agent, H_2O_2. For comparison, the experiments were conducted in the same condition of solution. The results are shown in Fig. 10. It was interesting to note that the degradation rate in the presence of both Bi_2WO_6 and H_2O_2 (10 mmol/L) was 1.95 times of the reaction rate by Bi_2WO_6 without using H_2O_2. However, H_2O_2 had no effect on the photocatalytic reaction without Bi_2WO_6.

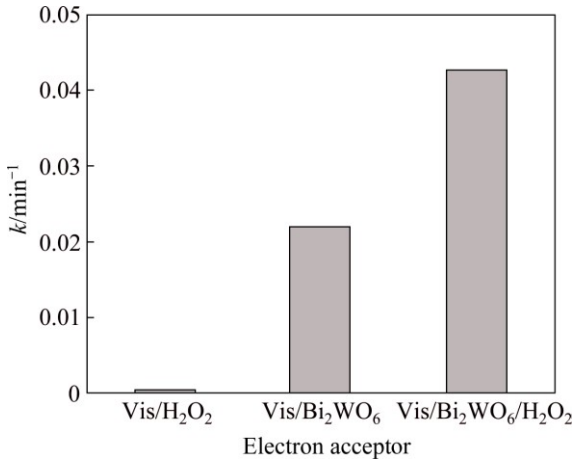

Fig. 10 Comparison of degradation rates of norfloxacin in photocatalytic reaction with or without 10 mmol/L H_2O_2 at Bi_2WO_6 dosage of 1 g/L, initial pH value of 9 and irradiation time of 60 min

$$H_2O_2+e_{cb}\longrightarrow \bullet OH+OH^- \quad (12)$$

Therefore, the application of H_2O_2 could markedly enhance the decomposition and mineralization of norfloxacin.

3.7 Photoluminescence

Figure 11 shows the room-temperature PL spectra of Bi_2WO_6 samples prepared at pH 4, 7, 9 and 11. All the prepared samples exhibit a broad emission peak at around 450 nm, which agrees with UV–Vis DRS analysis. Generally, a lower PL intensity is indicative of a higher separation rate of photogenerated carriers. Bi_2WO_6-pH4 shows relatively diminished PL intensity compared with Bi_2WO_6 samples prepared at pH 7, 9 and 11, indicating that the lower pH led to a greater increase in the inhibition of electron−hole recombination. This result might be derived from the fact that Bi_2WO_6 samples prepared at pH 4 had smaller nanoflakes, which was beneficial for promoting the carrier separation and therefore hindering the charge recombination.

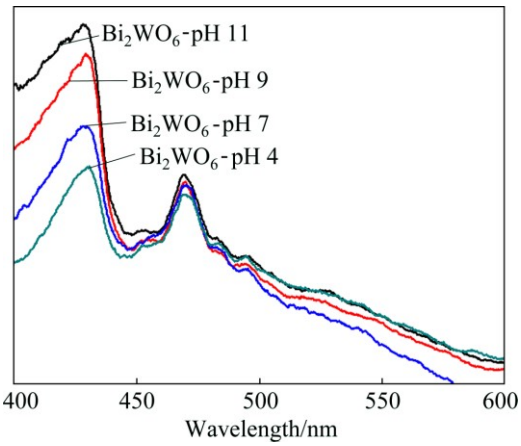

Fig. 11 Photoluminescence spectra of Bi_2WO_6 prepared at different pH values

4 Conclusions

The hydrothermally synthesized Bi_2WO_6 prepared at different pH exhibited different hierarchical architectures. The relationship between specific surface area and electron mobility had a great influence on photocatalytic activity of the photocatalyst. A low density of recombination centers and a large specific surface area were imperative factors for Bi_2WO_6 to gain a higher level of photocatalytic activity. Bi_2WO_6-pH4 was highly active for photocatalytic degradation of norfloxacin. The influences of dosage, initial

concentration and pH levels on the degradation performance were investigated. Slightly alkaline solution would improve the photocatalytic efficiency. As the norfloxacin concentration increased, the decrease of adsorption percentage and light penetration lowered the photocatalytic efficiency. The degradation rate of the pollutant could be enhanced by the addition of H_2O_2 as an electron acceptor. The results of these investigations clearly demonstrate the importance of different "size effect" of photocatalyst on degradation of norfloxacin.

References

[1] KUMMERER K. Pharmaceuticals in the environment: Sources, fate, effects and risks [M]. Berlin: Springer, 2008.

[2] HIRSCH R, TERNES T, HABERER K, KRATZ K L. Occurrence of antibiotics in the aquatic environment [J]. Science of the Total Environment, 1999, 225: 109−118.

[3] SORENSEN B H, NIELSEN S N, LANZKY P, INGERSLEV F, LUTZHOFT H H, JORGENSEN S. Occurrence, fate and effects of pharmaceutical substances in the environment — A review [J]. Chemosphere, 1998, 36: 357−393.

[4] NEU H C. The crisis in antibiotic resistance [J]. Science, 1992, 257: 1064−1073.

[5] DAUGHTON C G, TERNES T A. Pharmaceuticals and personal care products in the environment: Agents of subtle change? [J]. Environmental Health Perspectives, 1999, 107: 907−938.

[6] GOLET E M, ALDRE A C, HARTMANN A, TERNES T A, GIGER W. Trace determination of fluoroquinolone antibacterial agents in urban wastewater by solid-phase extraction and liquid chromatography with fluorescence detection [J]. Analytical Chemistry, 2001, 73: 3632−3638.

[7] HUANG Dan-lian, ZENG Guang-ming, FENG Chong-ling, HU Shuang, JIANG Xiao-yun, TANG Lin, SU Feng-feng, ZHANG Yu, ZENG Wei, LIU Hong-liang. Degradation of lead-contaminated lignocellulosic waste by phanerochaete chrysosporium and the reduction of lead toxicity [J]. Environmental Science and Technology, 2008, 42: 4946−4951.

[8] JONES O, VOULVOULIS N, LESTER J. Human pharmaceuticals in the aquatic environment—A review [J]. Environmental Technology, 2001, 22: 1383−1394.

[9] DENG Yao-cheng, TANG Lin, ZENG Guang-ming, ZHU Zhe-jing, YAN Min, ZHOU Yao-yu, WANG Jia-jia, LIU Ya-ni, WANG Jing-jing. Insight into highly efficient simultaneous photocatalytic removal of Cr(VI) and 2,4-diclorophenol under visible light irradiation by phosphorus doped porous ultrathin g-C_3N_4 nanosheets from aqueous media: Performance and mechanism [J]. Applied Catalysis B: Environmental, 2017, 203: 343−354.

[10] TERNES T A. Occurrence of drugs in German sewage treatment plants and rivers [J]. Water Research, 1998, 32: 3245−3260.

[11] TANG Lin, DENG Yao-cheng, ZENG Guang-ming, HU Wei, WANG Jia-jia, ZHOU Yao-yu, WANG Jing-jing, TANG Jing, FANG Wei. CdS/Cu_2S co-sensitized TiO_2 branched nanorod arrays of enhanced photoelectrochemical properties by forming nanoscale heterostructure [J]. Journal of Alloys and Compounds, 2016, 662: 516−527.

[12] HAQUE M, MUNEER M. Photodegradation of norfloxacin in aqueous suspensions of titanium dioxide [J]. Journal of Hazardous Materials, 2007, 145: 51−57.

[13] COKGOR E U, ALATON I A, KARAHAN O, DOGRUEL S, ORHON D. Biological treatability of raw and ozonated penicillin formulation effluent [J]. Journal of Hazardous Materials, 2004, 116: 159−166.

[14] GHAUCH A, BAYDOUN H, DERMEROPIAN P. Degradation of aqueous carbamazepine in ultrasonic Fe_0/H_2O_2 systems [J]. Chemical Engineering Journal, 2011, 172: 18−27.

[15] PELAER M, NOLAN N T, PILLAI S C, SEERY M K, FALARAS P, KONTOS A G, DUNLOP P S, HAMILTON J W, BYRNE J A, O'SHEA K. A review on the visible light active titanium dioxide photocatalysts for environmental applications [J]. Applied Catalysis B: Environmental, 2012, 125: 331−349.

[16] TANG Lin, ZENG Guang-ming, SHENG Guo-li, LI Yuan-ping, ZHANG Yi, HUANG Dan-lian. Rapid detection of picloram in agricultural field samples using a disposable immunomembrane-based electrochemical sensor [J]. Environmental Science and Technology, 2008, 42: 1207−1212.

[17] TANG Lin, FANG Yan, PANG Ya, ZENG Guang-ming, WANG Jia-jia, ZHOU Yao-yu, DENG Yao-cheng, YANG Gui-de, CAI Ye, CHEN Jun. Synergistic adsorption and reduction of hexavalent chromium using highly uniform polyaniline-magnetic mesoporous silica composite [J]. Chemical Engineering Journal, 2014, 254: 302−312.

[18] TANG L, YANG G D, ZENG G M, CAI Y, LI S S, ZHOU Y Y, PANG Y, LIU Y Y, ZHANG Y, LUNA B. Synergistic effect of iron doped ordered mesoporous carbon on adsorption-coupled reduction of hexavalent chromium and the relative mechanism study [J]. Chemical Engineering Journal, 2014, 239: 114−122.

[19] ZENG Guang-ming, LIU Yuan-yuan, TANG Lin, YANG Gui-de, PANG Ya, ZHANG Yi, ZHOU Yao-yu. Enhancement of Cd (II) adsorption by polyacrylic acid modified magnetic mesoporous carbon [J]. Chemical Engineering Journal, 2015, 259: 153−160.

[20] INGERSLEV F, TORANG L, LOKE M L, SORENSEN B H, NYHOLM N. Primary biodegradation of veterinary antibiotics in aerobic and anaerobic surface water simulation systems [J]. Chemosphere, 2001, 44: 865−872.

[21] PRADO N, OCHOA J, AMRANE A. Biodegradation and biosorption of tetracycline and tylosin antibiotics in activated sludge system [J]. Process Biochemistry, 2009, 44: 1302−1306.

[22] CHATTERJEE D, DASGUPTA S. Visible light induced photocatalytic degradation of organic pollutants [J]. Journal of Photochemistry and Photobiology C: Photochemistry Reviews, 2005, 6: 186−205.

[23] DENG Yao-cheng, TANG Lin, ZENG Guang-ming, WANG Jia-jia, ZHOU Yao-yu, WANG Jing-jing, TANG Jing, LIU Ya-ni, PENG Bo, CHEN Fei. Facile fabrication of a direct Z-scheme Ag_2CrO_4/g-C_3N_4 photocatalyst with enhanced visible light photocatalytic activity [J]. Journal of Molecular Catalysis A: Chemical, 2016, 421: 209−221.

[24] MA Yun-zhu, CHENG Fan, LIU Wen-sheng, WANG Juan, WANG Yi-kai. Research progress of Ag_3PO_4 based photocatalyst: Fundamentals and performance enhancement [J]. Transactions of Nonferrous Metals Society of China, 2015, 25: 112−121.

[25] DUAN Yu-lu, ZHOU Li-qi, XU Guo-fu, ZHANG Hui-ying, LI Xu , LIU Xiao-he. Preparation and characterization of ZnSe/CdSe core-shell microspheres [J]. Transactions of Nonferrous Metals Society of China, 2015, 25: 1559−1567.

[26] FUJISHIMA A, HASHIMOTO K, WATANABE T. TiO_2 photocatalysis: Fundamentals and applications [M]. Birmingham: BKC Incorporated, 1999.

[27] FUJISHIMA A, RAO T N, TRYK D A. Titanium dioxide photocatalysis [J]. J Photochem Photobio C: Photochem Reviews, 2000, 1: 1−21.

[28] DENG Yao-cheng, TANG Lin, ZENG Guang-ming, DONG Hao-ran, YAN Ming, WANG Jing-jing, HU Wei, WANG Jia-jia, ZHOU Yao-yu, TANG Jing. Enhanced visible light photocatalytic performance of polyaniline modified mesoporous single crystal TiO_2 microsphere [J]. Applied Surface Science, 2016, 387: 882−8935.

[29] YU H, AI Z H, HO W K, CHEN M J, LEE S C. Ultrasonic spray pyrolysis synthesis of porous Bi_2WO_6 microspheres and their visible-light-induced photocatalytic removal of NO [J]. Journal of Physical Chemistry C, 2010, 114: 6342−6349.

[30] AMANO F, YAMAKATA A, NOGAMI K, OSAWA M, OHTANI B. Effect of photoexcited electron dynamics on photocatalytic efficiency of bismuth tungstate [J]. Journal of Physical Chemistry C, 2011, 115: 16598−16605.

[31] TANG Lin, WANG Jia-jia, ZENG Guang-ming, LIU Ya-ni, DENG Yao-cheng, ZHOU Yao-yu, TANG Jing, WANG Jing-jing, GUO Zhi. Enhanced photocatalytic degradation of norfloxacin in aqueous Bi_2WO_6 dispersions containing nonionic surfactant under visible light irradiation [J]. Journal of Hazardous Materials, 2016, 306: 295−304.

[32] SORGEL F, KINZIG M. Pharmacokinetics of gyrase inhibitors. Part 2: Renal and hepatic elimination pathways and drug interactions [J]. The American Journal of Medicine, 1993, 94: 56−69.

[33] WANG Chun-ying, ZHANG Hao, LI Fang, ZHU Ling-yan. Degradation and mineralization of bisphenol A by mesoporous Bi_2WO_6 under simulated solar light irradiation [J]. Environmental Science and Technology, 2010, 44: 6843−6848.

[34] WANG Chun-ying, ZHU Ling-yan, SONG Chao, SHAN Guo-qiang, CHEN Peng. Characterization of photocatalyst $Bi_{3.84}W_{0.16}O_{6.24}$ and its photodegradation on bisphenol A under simulated solar light irradiation [J]. Applied Catalysis B: Environmental, 2011, 105: 229−236.

[35] YU Shu-hong, LIU Biao, MO Mao-song, HUANG Jina-hua, LIU Xian-ming, QIAN Yi-tai. General synthesis of single-crystal tungstate nanorods/nanowires: A facile, low-temperature solution approach [J]. Advanced Functional Materials, 2003, 13: 639−647.

[36] TIAN Yue, HUA Guo-min, XU Wei, LI Nian, FANG Ming, ZHANG Li-de. Bismuth tungstate nano/microstructures: Controllable morphologies, growth mechanism and photocatalytic properties [J]. Journal of Alloys and Compounds, 2011, 509: 724−730.

[37] ZHANG Li-sha, WANG Wen-zhong, ZHOU Lin, XU Hao-lan. Bi_2WO_6 nano-and microstructures: Shape control and associated visible-light- driven photocatalytic activities [J]. Small, 2007, 3(9): 1618−1625.

[38] XIE Hui-dong, SHEN De-zhong, WANG Xiao-qing, SHENG Guang-qiu. Growth and characterization of $KBi(WO_4)_2$ single crystals [J]. Journal of Crystal Growth, 2008, 310: 2550−2554.

[39] KUDO A, TSUJI I, KATO H. $AgInZn_7S_9$ solid solution photocatalyst for H_2 evolution from aqueous solutions under visible light irradiation [J]. Chemical Communications, 2002, 17: 1958−1959.

[40] OLLIS D F. Contaminant degradation in water [J]. Environmental Science and Technology, 1985, 19: 480−484.

[41] CHEN Peng, ZHU Ling-yan, FANG Shu-hong, WANG Chun-ying, SHAN Guo-qiang. Photocatalytic degradation efficiency and mechanism of microcystin-RR by mesoporous Bi_2WO_6 under near ultraviolet light [J]. Environmental Science and Technology, 2012, 46: 2345−2351.

[42] OHTANI B, IWAI K, KOMINAMI H, MATSUURA T, KERA Y, NISHIMOTO S I. Titanium (IV) oxide photocatalyst of ultra-high activity for selective N-cyclization of an amino acid in aqueous suspensions [J]. Chemical Physics Letters, 1995, 242: 315−319.

[43] ALLOUNI Z E, CIMPAN M R, HØL P J, SKODVIN T, GJERDET N R. Agglomeration and sedimentation of TiO_2 nanoparticles in cell culture medium [J]. Colloids and Surfaces B: Biointerfaces, 2009, 68: 83−87.

[44] PETERSON M, TURNER J, NOZIK A. Mechanistic studies of the photocatalytic behavior of titania: Particles in a photoelectrochemical slurry cell and the relevance to photodetoxification reactions [J]. Journal of Physical Chemistry, 1991, 95: 221−225.

[45] KIM D H, ANDERSON M A. Solution factors affecting the photocatalytic and photoelectrocatalytic degradation of formic acid using supported TiO_2 thin films [J]. Journal of Photochemistry and Photobiology A: Chemistry, 1996, 94: 221−229.

[46] FU Hong-bo, PAN Cheng-si, YAO Wen-qing, ZHU Yong-fa. Visible-light-induced degradation of Rhodamine B by nanosized Bi_2WO_6 [J]. Journal of Physical Chemistry B, 2005, 109: 22432−22439.

[47] WANG Ya-jun, BAI Xiao-juan, PAN Cheng-si, HE Jun, ZHU Yong-fa. Enhancement of photocatalytic activity of Bi_2WO_6 hybridized with graphite-like C_3N_4 [J]. Journal of Materials Chemistry C, 2012, 22: 11568−11573.

[48] YAMADA Y, NOMURA A, MIYAHIGASHI T, FUKUZUMI S. Photocatalytic production of hydrogen peroxide by two-electron reduction of dioxygen with carbon-neutral oxalate using a 2-phenyl-4-(1-naphthyl) quinolinium ion as a robust photocatalyst [J]. Chemical Communications, 2012, 48: 8329−8331.

不同分层体系结构钨酸铋对可见光催化降解诺氟沙星的影响

王佳佳[1,2]，汤 琳[1,2]，曾光明[1,2]，周耀渝[3]，邓垚成[1,2]，范长征[1,2]，龚继来[1,2]，刘雅妮[1,2]

1. 湖南大学 环境科学与工程学院，长沙 410082；
2. 湖南大学 环境生物与污染控制教育部重点实验室，长沙 410082；
3. 湖南农业大学 资源环境学院，长沙 410128

摘 要：研究不同分层体系结构钨酸铋对可见光催化降解诺氟沙星的影响。在 pH 值为 4~11 条件下采用水热法反应合成钨酸铋。结果表明：在 pH 值为 4 条件下制备的钨酸铋对诺氟沙星具有很好的吸附和光催化性能。表征结果显示，pH 值为 4 时制备的钨酸铋具有较大的比表面积和光生载流子分离效率。在弱碱条件下，催化降解速率达到最大，这是由于弱碱溶液提供了足量的 OH^-，光子与材料表面吸附的 OH^-反应生成了羟基自由基。本实验证明，较小尺寸的超薄钨酸铋是一种有效的诺氟星沙污染水体光催化剂。

关键词：诺氟沙星；钨酸铋；分层体系结构；光催化降解；尺寸效应

(Edited by Wei-ping CHEN)